

ON ORTHOGONAL PROJECTIONS FOR DIMENSION REDUCTION AND APPLICATIONS IN VARIATIONAL LOSS FUNCTIONS FOR LEARNING PROBLEMS

A. BREGER¹, J. I. ORLANDO², P. HARAR³, M. DÖRFLER¹, S. KLIMSCHA²,
C. GRECHENIG², B. S. GERENDAS^{1,2}, U. SCHMIDT-ERFURTH², AND M. EHLER¹

ABSTRACT. The use of orthogonal projections on high-dimensional input and target data in learning frameworks is studied. First, we investigate the relations between two standard objectives in dimension reduction, maximizing variance and preservation of pairwise relative distances. The derivation of their asymptotic correlation and numerical experiments tell that a projection usually cannot satisfy both objectives. In a standard classification problem we determine projections on the input data that balance them and compare subsequent results. Next, we extend our application of orthogonal projections to deep learning frameworks. We introduce new variational loss functions that enable integration of additional information via transformations and projections of the target data. In two supervised learning problems, clinical image segmentation and music information classification, the application of the proposed loss functions increase the accuracy.

1. INTRODUCTION

Linear dimension reduction is commonly used for preprocessing of high-dimensional data in complicated learning frameworks to compress and weight important data features. Conventional approaches apply specific projections that preserve essential information and complexity within a more compact representation. The projector is usually selected by optimizing distinct objectives, such as maximization of the sample variance or preservation of pairwise relative distances. Widely used orthogonal projections for dimension reduction are variants of the principal component analysis (PCA) that maximize the variance of the projected data. Preservation of relative pairwise distances asks for a near-isometric embedding, and random projections guarantee this embeddings with high probability, cf. [12, 5] and see also [1, 27, 4, 10, 24, 23].

In the present manuscript, we aim to better understand the interplay between the following two objectives in learning frameworks:

- O1) maximizing variance (PCA),
- O2) preservation of pairwise relative distances (random projections).

(1) UNIVERSITY OF VIENNA, DEPARTMENT OF MATHEMATICS, VIENNA, AUSTRIA

(2) MEDICAL UNIVERSITY OF VIENNA, DEPARTMENT OF OPHTHALMOLOGY, VIENNA, AUSTRIA

(3) BRNO UNIVERSITY OF TECHNOLOGY, DEPARTMENT OF TELECOMMUNICATIONS, BRNO, CZECH REPUBLIC

We achieve the following goals: first we clarify mathematically and numerically that the two objectives are competing. Depending on the dimensions we heuristically determine beneficial choices and numerically find a balancing projector for a given data set. Finally, we introduce a variational loss function for deep neural networks, that integrates additional output/target information via features and projections. We observe that our proposed methodology can increase the accuracy in two deep learning problems.

In contrast to conventional approaches we study the joint behavior of the two objectives with respect to the entire set of orthogonal projectors. By analyzing the correlation between the variance and pairwise relative distances of projected data, we observe that O1) and O2) are competing and usually cannot be reached at the same time. In numerical learning experiments we investigate heuristic choices of projections, applied to input features for subsequent classification with support vector machine and shallow neural networks.

In view of deep learning frameworks, we utilize features and projections on target data. We propose a modified variational loss function, in which suitable transformations and projections provide beneficial representations of the target space. It is applied in two supervised deep learning problems dealing with real world data.

The first experiment is a clinical image segmentation problem in optical coherence tomography (OCT) data of the human retina. Related principles of dimension reduction for other clinical classification problems in OCT have already been successfully applied in [7]. In the second experiment we aim to categorize musical instruments based on their spectrogram, see [16] for related results. Our proposed variational loss function can increase the accuracy in both experiments.

The outline is as follows. In Section 2 we address the analysis of the competing objectives and Theorem 2.5 yields the asymptotic correlation between variance and pairwise relative distances of projected data. Section 3 prepares for the numerical investigations by recalling t -designs as considered in [8], enabling subsequent numerics. Heuristic investigations on projected input used in a classification task, are presented in Section 4. The modified variational loss function is introduced in Section 5. Finally, in Sections 6 and 7 we present the classification experiments on OCT images and musical instruments.

2. DIMENSION REDUCTION WITH ORTHOGONAL PROJECTIONS

To reduce the dimension of a high-dimensional data set $x = \{x_i\}_{i=1}^m \subset \mathbb{R}^d$, we map x into a lower-dimensional affine linear subspace $\bar{x} + V$, where $\bar{x} := \frac{1}{m} \sum_{i=1}^m x_i$ is the sample mean and V is a k -dimensional linear subspace of \mathbb{R}^d with $k < d$. This mapping is performed by an orthogonal projector $p \in \mathcal{G}_{k,d}$, where

$$\mathcal{G}_{k,d} := \{p \in \mathbb{R}^{d \times d} : p^2 = p, p^\top = p, \text{rank}(p) = k\}$$

denotes the Grassmannian, so that the lower-dimensional data representation is

$$(2.1) \quad \{\bar{x} + p(x_i - \bar{x})\}_{i=1}^m \in \bar{x} + V,$$

with $\text{range}(p) = V$. The optimal choice of p within $\mathcal{G}_{k,d}$ depends on further objectives. In the following, we consider two objectives associated to popular choices of orthogonal projectors for dimension reduction, in particular random projectors and PCA. We will first observe that the two underlying objectives are competing, especially in high dimensions, and then discuss consequences.

2.1. Objective O1). The total sample variance¹ $\text{tvar}(x)$ of $x = \{x_i\}_{i=1}^m \subset \mathbb{R}^d$ is the sum of the corrected variances along each dimension, i.e. can be written by

$$(2.2) \quad \text{tvar}(x) := \frac{1}{m-1} \sum_{i=1}^m \|x_i - \bar{x}\|^2.$$

PCA aims to construct $p \in \mathcal{G}_{k,d}$, such that the total sample variance of (2.1) is maximized among all projectors in $\mathcal{G}_{k,d}$.

The total sample variance of $px = \{px_i\}_{i=1}^m$ coincides with the one of (2.1) and satisfies

$$\text{tvar}(px) \leq \text{tvar}(x)$$

for all $p \in \mathcal{G}_{k,d}$. Thus, PCA achieves optimal variance preservation. The total variance (2.2) can be expressed via pairwise distances

$$(2.3) \quad \text{tvar}(x) = \frac{1}{m(m-1)} \sum_{i < j} \|x_i - x_j\|^2.$$

Equally, it holds that

$$(2.4) \quad \text{tvar}(px) = \frac{1}{m(m-1)} \sum_{i < j} \|p(x_i) - p(x_j)\|^2,$$

which reveals that PCA maximizes the sample mean of the projected pairwise distances and therefore favors preservation of large distances.

2.2. Objective O2). In contrast to pairwise absolute distances, the Johnson-Lindenstrauss Lemma targets the preservation of pairwise relative distances:

Lemma 2.1 (Johnson-Lindenstrauss, cf. [12, 27]). *For any $0 < \epsilon < 1$, any $m, k, d \in \mathbb{N}$ with*

$$\frac{4 \log(m)}{\epsilon^2/2 - \epsilon^3/3} \leq k \leq d,$$

and any $\{x_i\}_{i=1}^m \subset \mathbb{R}^d$, there is a projector $p \in \mathcal{G}_{k,d}$ such that

$$(2.5) \quad (1 - \epsilon) \|x_i - x_j\|^2 \leq \frac{d}{k} \|p(x_i) - p(x_j)\|^2 \leq (1 + \epsilon) \|x_i - x_j\|^2, \quad i < j.$$

For small $\epsilon > 0$, the projector p in Lemma 2.1 yields that all of the $\frac{m(m-1)}{2}$ pairwise relative distances

$$(2.6) \quad \left\{ \frac{d}{k} \frac{\|p(x_i) - p(x_j)\|^2}{\|x_i - x_j\|^2} : i < j \right\}$$

are close to 1, i.e. the projection p preserves all scaled pairwise relative distances well. A good choice of p in Lemma 2.1 is based on random projectors

¹We use lower case letters for samples and upper case letters for random vectors/matrices.

$P \sim \lambda_{k,d}$, where $\lambda_{k,d}$ denotes the unique orthogonally invariant probability measure on $\mathcal{G}_{k,d}$. The following Theorem is essentially proved by following the lines of the proof of Lemma 2.1 in [12] after replacing the constant 4 with $(2 + \tau)2$ in the respective bound on k .

Theorem 2.2. *For any $0 < \epsilon < 1$, any $m, k, d \in \mathbb{N}$ and any $0 < \tau$ with*

$$\frac{(2 + \tau)2 \log(m)}{\epsilon^2/2 - \epsilon^3/3} \leq k \leq d,$$

and any $\{x_i\}_{i=1}^m \subset \mathbb{R}^d$, the random projector $P \sim \lambda_{k,d}$ satisfies

$$(2.7) \quad \left\{ \frac{d \|P(x_i) - P(x_j)\|^2}{k \|x_i - x_j\|^2} : i < j \right\} \in [1 - \epsilon, 1 + \epsilon]$$

with probability at least $(1 - \frac{1}{m^\tau} + \frac{1}{m^{\tau+1}})$.

2.3. Competing objectives. The near-isometry property (2.5) implies

$$(1 - \epsilon) \frac{k}{d} \text{tvar}(x) \leq \text{tvar}(px) \leq (1 + \epsilon) \frac{k}{d} \text{tvar}(x),$$

so that the total variance of the projected data px cannot be maximized for $k < d$. In particular, with high probability a random projector $P \sim \lambda_{k,d}$ does not suit the objective of maximizing the total variance, and we even have $\mathbb{E} \text{tvar}(Px) = \frac{k}{d} \text{tvar}(x)$, see (A.2) in the appendix. On the other hand, the PCA projector is not generally suited for preservation of pairwise relative distances as it treats larger and smaller distances differently. The preservation of larger distances is favored since PCA maximizes (2.4) among all $p \in \mathcal{G}_{k,d}$, cf. [31], and $\|p(x_i) - p(x_j)\| \leq \|x_i - x_j\|$ holds for all $i < j$. Distinct points could be projected onto a single point and pairwise distances may be distorted, e.g. when data lies on a nonlinear manifold. Preserving the geometrical structure is often important for subsequent classification tasks.

To quantitatively understand the relation between the two competing objectives, we consider the sample mean and the uncorrected sample variance of the pairwise relative distance (2.6),

$$(2.8) \quad \mathcal{M}(p, x) := \frac{2}{m(m-1)} \sum_{i < j} \frac{d \|p(x_i - x_j)\|^2}{k \|x_i - x_j\|^2},$$

$$(2.9) \quad \mathcal{V}(p, x) := \frac{2}{m(m-1)} \sum_{i < j} \frac{d^2 \|p(x_i - x_j)\|^4}{k^2 \|x_i - x_j\|^4} - \mathcal{M}(p, x)^2.$$

Recall that good preservation of the relative pairwise distances in (2.6) asks for $\mathcal{M}(p, x)$ being close to 1 and the variance $\mathcal{V}(p, x)$ being small. In the following, we analyze $\text{tvar}(px)$, $\mathcal{M}(p, x)$, and $\mathcal{V}(p, x)$ and their expectations for random $P \in \mathcal{G}_{k,d}$.

In Figure 2.1 we see a simple numerical experiment, where we first create a normal distributed fixed data set $\{x_i\}_{i=1}^m$ with $x_i \in \mathbb{R}^d$ for $i = 1, \dots, m$ and $m = 100$, $d = 50$. We then compute $n = 10000$ random projections p , distributed according to $\lambda_{k,50}$ and also PCA for $k = 10, 20, 30, 40$. In Figure 2.1 (a) - (d) we can see that the more k differs from d , the more PCA and random projections differ concerning $\text{tvar}(px)$ and $\mathcal{M}(p, x)$. Their different actions on the data may yield very diverse behavior in subsequent

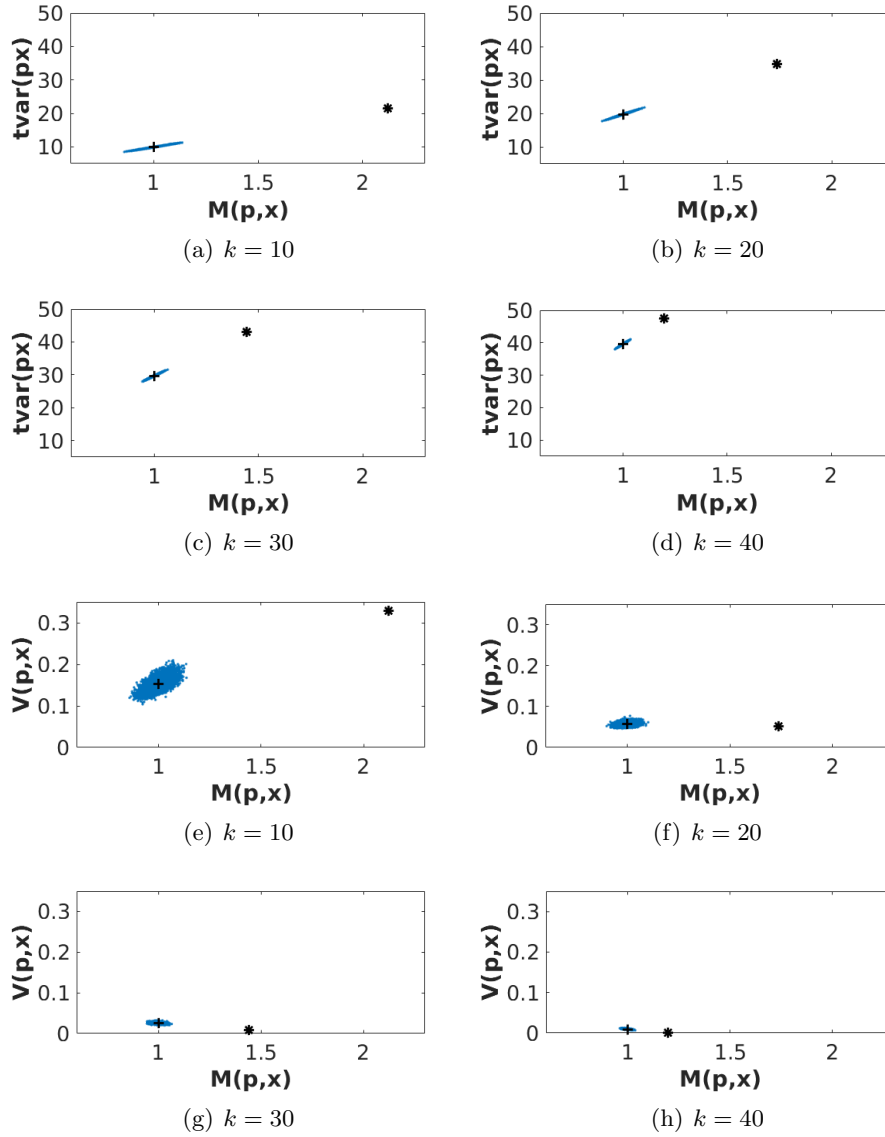


FIGURE 2.1. Competing properties: 10000 random projections $p \sim \lambda_{k,50}$ versus PCA (*), plotted concerning $tvar(px)$, $\mathcal{M}(p, x)$ and $\mathcal{V}(p, x)$. The normal distributed fixed data set x has total variance $tvar(x) = 49.5$. Random projections cluster around their expectation values (2.10), (2.11) and (2.12), marked by +.

analysis. Moreover, we compare $\mathcal{M}(p, x)$ and $\mathcal{V}(p, x)$ in Figure 2.1 (e) - (h) for the different k . We can see that again when k is much smaller than d , random projections and PCA differ more concerning the variance of pairwise distances $\mathcal{V}(p, x)$. For $k = 10$ the variance for PCA is higher in comparison to random projections, see Figure 2.1 (e), for $k = 40$ vice versa, see Figure 2.1 (h).

Remark 2.3. To balance the two objectives O1) and O2) we suggest to favor PCA when $k \gg d/2$ and to select random projectors when $k \ll d/2$. For $k \gg d/2$ PCA loses very little information, whereas for $k \ll d/2$ it cannot yield high total variance and loses more information of pairwise distances. The case $k \approx d/2$ shall be investigated more closely.

2.4. Covariances and correlation between competing objectives.

For further mathematical analysis we first introduce a more general class of probability measures on $\mathcal{G}_{k,d}$ that resemble $\lambda_{k,d}$ sufficiently well:

Definition 2.4. A Borel probability measure λ on $\mathcal{G}_{k,d}$ is called a cubature measure of strength t if

$$\int_{\mathcal{G}_{k,d}} f(p) d\lambda_{k,d}(p) = \int_{\mathcal{G}_{k,d}} f(p) d\lambda(p), \quad \text{for all } f \in \text{Pol}_t(\mathbb{R}^{d \times d}),$$

where $\text{Pol}_t(\mathbb{R}^{d \times d})$ denotes the set of multivariate polynomials of total degree t in d^2 variables.

For random P , we now determine the expectation values for our 3 quantities of interest: $\text{tvar}(Px)$, $\mathcal{M}(P, x)$, and $\mathcal{V}(P, x)$. If $P \sim \lambda$ and λ is a cubature measure of strength at least 2, the identities (A.2) and (A.3) in the appendix and a short calculation yield

$$(2.10) \quad \mathbb{E} \text{tvar}(Px) = \frac{k}{d} \text{tvar}(x),$$

$$(2.11) \quad \mathbb{E} \mathcal{M}(P, x) = 1,$$

$$(2.12) \quad \mathbb{E} \mathcal{V}(P, x) = a_{k,d} \left(1 - \frac{4}{m^2(m-1)^2} \sum_{\substack{i < j \\ l < r}} \langle \frac{x_i - x_j}{\|x_i - x_j\|}, \frac{x_l - x_r}{\|x_l - x_r\|} \rangle^2 \right),$$

where $a_{k,d} = \frac{2d(d-k)}{k(d-1)(d+2)}$. The expected sample variance in (2.12) satisfies

$$\mathbb{E} \mathcal{V}(P, x) \leq a_{k,d} \longrightarrow \frac{2}{k}, \quad \text{for } d \rightarrow \infty.$$

This asymptotic bound relates to Theorem 2.2 and alludes to a near-isometry property of the type (2.7) for k sufficiently large.

The following Theorem 2.5 provides a lower bound for random P on the population correlation

$$(2.13) \quad \text{Corr}(\mathcal{M}(P, x), \text{tvar}(Px)) = \frac{\text{Cov}(\mathcal{M}(P, x), \text{tvar}(Px))}{\sqrt{\text{Var}(\mathcal{M}(P, x))} \sqrt{\text{Var}(\text{tvar}(Px))}}.$$

It holds for arbitrary dimensions d and subsequently specifies the asymptotic behavior for $d \rightarrow \infty$:

Theorem 2.5. Let $x = \{x_i\}_{i=1}^m \subset \mathbb{R}^d$ be pairwise different and let $P \sim \lambda$, with λ being a cubature measure of strength at least 2. For $d \geq \frac{m(m-1)}{2}$, the correlation (2.13) is bounded from below by

$$(2.14) \quad \frac{\min_{i \neq j} \|x_i - x_j\|^2}{\max_{i \neq j} \|x_i - x_j\|^2} - \frac{m(m-1)}{2d} \cdot \frac{\max_{i \neq j} \|x_i - x_j\|^2}{\min_{i \neq j} \|x_i - x_j\|^2}.$$

Let $\{x_i\}_{i=1}^m \subset \mathbb{R}^d$ be random points, whose entries are independent, identically distributed with finite 4-th moments, that are uniformly bounded in d . Then (2.14) converges towards 1 in probability for $d \rightarrow \infty$.

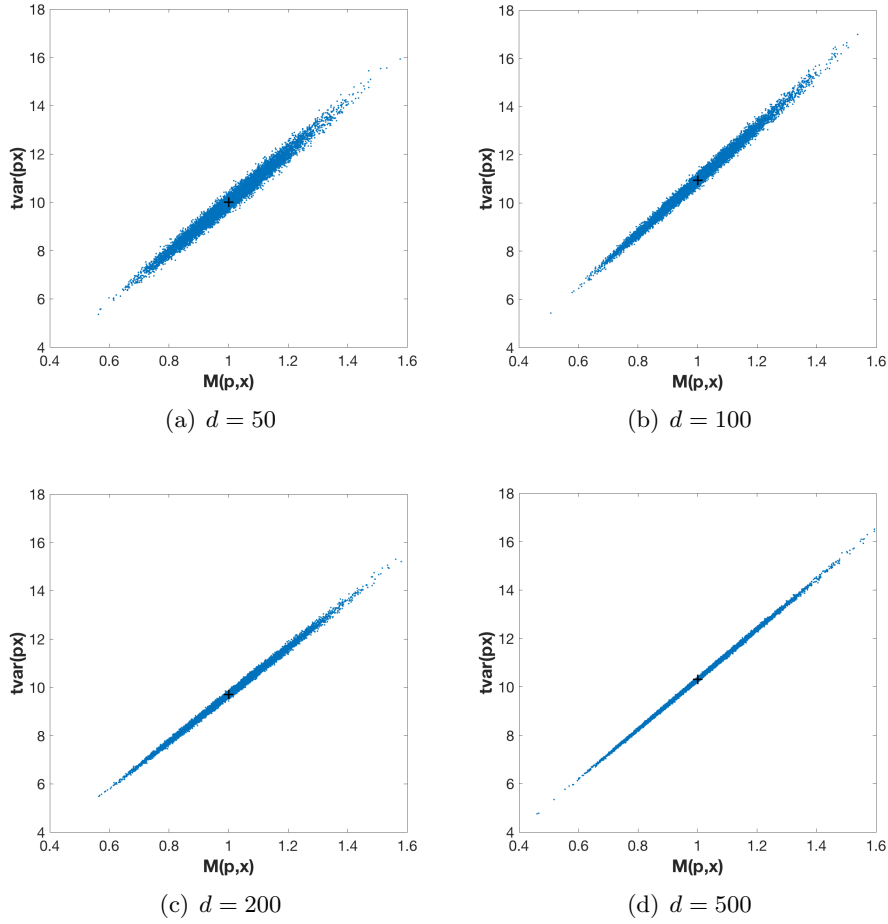


FIGURE 2.2. For $x = \{x_i\}_{i=1}^{10} \in \mathbb{R}^d$ with independent, normal distributed entries, we independently sample 10000 random projectors p from $\lambda_{10,d}$ and plot $\mathcal{M}(p, x)$ versus $\text{tvar}(px)$. The expectation values with respect to $P \sim \lambda$ are marked with $+$. The correlation is already 0.9916 for $d = 50$ and grows further when d increases, namely with values 0.9961, 0.9985, 0.9996 for $d = 100, 200, 500$.

The strong correlation for large dimensions d in the second part of Theorem 2.5 suggests that increasing $\text{tvar}(Px)$ may also lead to increasing $\mathcal{M}(P, x)$, see Figure 2.2 for illustration. Thus, large projected total variance $\text{tvar}(Px)$ and the preservation of scaled pairwise distances, i.e. $\mathcal{M}(P, x)$ being close to 1, are competing properties. Whether a random projector favoring pairwise relative distances or PCA favoring maximal variance is beneficial depends on the particular data analysis task. It seems reasonable that often projections balancing both objectives are preferable.

Note that the second part of Theorem 2.5 relates to the well-known fact that random vectors in high dimensions are almost orthogonal. Standard concentration of measure arguments may lead to more quantitative versions.

3. PREPARATIONS FOR NUMERICAL EXPERIMENTS

For the numerical experiments we need finite sets of projectors that represent the overall space well, i.e. cover $\mathcal{G}_{k,d}$ properly.

3.1. Optimal covering sequences. Let the *covering radius* $\{p_l\}_{l=1}^n \subset \mathcal{G}_{k,d}$ be denoted by

$$(3.1) \quad \varrho(\{p_l\}_{l=1}^n) := \sup_{p \in \mathcal{G}_{k,d}} \min_{1 \leq l \leq n} \|p - p_l\|_F,$$

where $\|\cdot\|_F$ is the Frobenius norm. The smaller the covering radius the better the covering. Following Lemma 2.1 we can connect finite sets of projections and their covering radius to the near-isometry property:

Lemma 3.1. *Let $\{p_l\}_{l=1}^n \subset \mathcal{G}_{k,d}$ and denote $\varrho := \varrho(\{p_l\}_{l=1}^n)$. For any $0 < \epsilon < 1$, any $m, k, d \in \mathbb{N}$ with*

$$\frac{4 \log(m)}{\epsilon^2/2 - \epsilon^3/3} \leq k \leq d,$$

and any $\{x_i\}_{i=1}^m \subset \mathbb{R}^d$, there is $l_0 \in \{1, \dots, n\}$ such that

$$(3.2) \quad (1 - \delta) \|x_i - x_j\|^2 \leq \frac{d}{k} \|p_{l_0}(x_i) - p_{l_0}(x_j)\|^2 \leq (1 + \delta) \|x_i - x_j\|^2, \quad i < j,$$

where $\delta = \epsilon + 2\varrho \sqrt{\frac{(1+\epsilon)d}{k}} + \frac{d}{k} \varrho^2$.

Proof. Given an arbitrary projector $p \in \mathcal{G}_{k,d}$, there is an index $l_0 \in \{1, \dots, n\}$ such that

$$\|p_{l_0}x - px\| \leq \|p_{l_0} - p\|_F \|x\| \leq \varrho \|x\|, \quad x \in \mathbb{R}^d.$$

From here, standard computations imply Lemma 3.1. We omit the details. \blacksquare

The accuracy of the near-isometry property in (3.2) depends on the covering radius. Therefore, a set $\{p_l\}_{l=1}^n \in \mathcal{G}_{k,d}$ with a small covering radius ϱ is more likely to contain a projector with better preservation of pairwise relative distances. According to [9], it holds that ¹ $\varrho \gtrsim n^{-\frac{1}{k(d-k)}}$, and we shall see next, how to achieve this lower bound.

A set of projectors $\{p_l\}_{l=1}^n \subset \mathcal{G}_{k,d}$ is called a *t-design* if the associated normalized counting measure $\frac{1}{n} \sum_{l=1}^n \delta_{p_l}$ is a cubature measure of strength t (see Definition 2.4). Any sequence of t_i -designs $\{p_l^i\}_{l=1}^{n_i} \subset \mathcal{G}_{k,d}$ with $t_i \rightarrow \infty$ satisfies

$$(3.3) \quad \varrho_i \asymp t_i^{-1},$$

and moreover, the bound $n_i \gtrsim t_i^{k(d-k)}$ holds, cf. [14, 9]. To relate n_i with ϱ_i via t_i , a sequence of t_i -designs $\{p_l^i\}_{l=1}^{n_i} \subset \mathcal{G}_{k,d}$ is called a *low-cardinality design sequence* if $t_i \rightarrow \infty$ and

$$(3.4) \quad n_i \asymp t_i^{k(d-k)}, \quad i = 1, 2, \dots$$

¹We use the symbols \lesssim and \gtrsim to indicate that the corresponding inequalities hold up to a positive constant factor on the respective right-hand side. The notation \asymp means that both relations \lesssim and \gtrsim hold.

For their existence and numerical constructions, we refer to [19] and [8, 9]. According to [9], see also (3.3) and (3.4), any low-cardinality design sequence $\{p_l^i\}_{l=1}^{n_i}$ covers asymptotically optimal, i.e.,

$$q_i \asymp n_i^{-\frac{1}{k(d-k)}}.$$

Benefiting from the covering property, we will use low-cardinality design sequences as a representation of the overall space of orthogonal projectors $\mathcal{G}_{k,d}$.

3.2. Linear least squares fit. With the linear least squares fit we can directly gain information about the relation between $\mathcal{M}(p, x)$ and $\text{tvar}(px)$ for a given data set $x = \{x_i\}_{i=1}^m \subset \mathbb{R}^d$ when p varies. Given the two samples

$$(3.5) \quad \{\text{tvar}(p_1x), \dots, \text{tvar}(p_nx)\}, \quad \{\mathcal{M}(p_1, x), \dots, \mathcal{M}(p_n, x)\},$$

the linear least squares fitting provides the best fitting straight line,

$$\text{tvar}(p_lx) \approx s \cdot \mathcal{M}(p_l, x) + \gamma, \quad l = 1, \dots, n,$$

where s and γ are determined by the sample variances and the sample covariance. If $\{p_l\}_{l=1}^n$ is a 2-design, then the sample (co)variances coincide with the respective population (co)variances for $P \sim \lambda_{k,d}$. Please see Appendix A.3 for further details. It follows that

$$(3.6) \quad s = \frac{\text{Cov}(\mathcal{M}(P, x), \text{tvar}(Px))}{\text{Var}(\mathcal{M}(P, x))} \quad \text{with } P \sim \lambda_{k,d},$$

$$(3.7) \quad \gamma = \frac{k}{d} \text{tvar}(x) - s.$$

The quantities s and γ can be directly computed, where $\text{tvar}(x)$ is given by (2.2) and the covariances are stated in Corollary A.1. Note that (3.6) and (3.7) are now independent of the particular choice of $\{p_l\}_{l=1}^n$.

The correlation between the two samples (3.5) yields additional information about their relation. As before, if $\{p_l\}_{l=1}^n$ is a 2-design, then the sample correlation coincides with the population correlation (2.13) for $P \sim \lambda_{k,d}$, cf. Appendix A.3. In particular if $k \approx d/2$, high correlation for a specific data set x suggests that random projections and PCA preserve competing properties, whose benefits need to be assessed for the specific subsequent task.

4. NUMERICAL EXPERIMENTS IN PATTERN RECOGNITION

We shall investigate the classification results of specific orthogonal projections applied to input data that is subsequently classified with simple learning frameworks. Projectors are chosen from a t -design in view of $\text{tvar}(px)$ and $\mathcal{M}(p, x)$. For all computations made in this Section the ‘Neural Network’ and ‘Statistics and Machine Learning’ toolboxes in MatlabR2017a are used.

We use the publicly available `iris` data set from the UCI Repository of Machine Learning Database suitable for supervised classification learning. It consists of 3 classes with 50 instances each, where each class refers to a type of iris plant. The instances are described by 4 features resulting in the input samples $\{x_i\}_{i=1}^{150} \subset \mathbb{R}^4$ and target samples $\{y_i\}_{i=1}^{150} \subset \{0, 1\}^3$. For

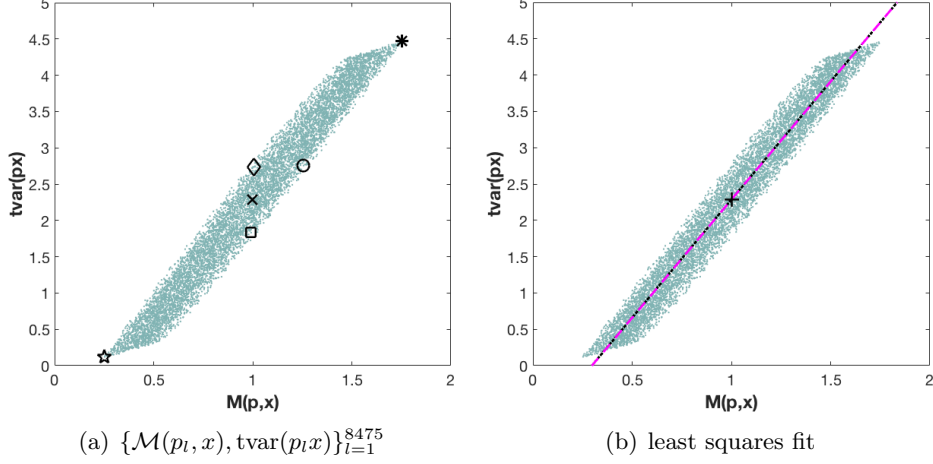


FIGURE 4.1. Projections $\{p_l\}_{l=1}^{8475} \subset G_{2,4}$ from a t-design of strength 14 evaluated on the iris data set $x \in \mathbb{R}^{4 \times 150}$.

comparison we classify the diverse input data with support vector machine (SVM) and 3-layer neural networks (NN) with 5 and 10 hidden units (HU).

4.1. Choice of orthogonal projection. In the experiment we use projections $p \in \mathcal{G}_{2,4}$ reducing the original dimension from $d = 4$ to $k = 2$. As a finite representation of the overall space, we use a t-design of strength 14 from a low-cardinality sequence (see Section 3.1) consisting of 8475 orthogonal projectors. Note that the dimension reduction in practice takes place by applying $q \in \mathcal{V}_{k,d}$ with $q^\top q = p \in \mathcal{G}_{k,d}$, where

$$\mathcal{V}_{k,d} := \{q \in \mathbb{R}^{k \times d} : qq^\top = I_k\}$$

denotes the Stiefel manifold. When taking norms, p and q are interchangeable, i.e., $\|q(x)\|^2 = \|p(x)\|^2$, for all $x \in \mathbb{R}^d$. Therefore we can use w.l.o.g. the theory developed for p .

The projections are chosen in a deterministic manner viewing the previously described competing properties. In Figure 4.1 the three quantities $\text{tvar}(px)$, $\mathcal{M}(p, x)$ and $\mathcal{V}(p, x)$ are pairwise plotted for all projectors in $\{p_l\}_{l=1}^{8475}$. For comparison we choose the following projections $p \in \{p_l\}_{l=1}^{8475} \subset \mathcal{G}_{2,4}$, see Figure 4.1(a) for a visualization.

- p_\times closest to the expected values 1 and $\frac{k}{d} \text{tvar}(x)$ (see (2.10) and (2.11)),
- p_\diamond preserving $\mathcal{M}(p, x) \approx 1$ and maximizing $\text{tvar}(px)$,
- p_\square preserving $\mathcal{M}(p, x) \approx 1$ and minimizing $\text{tvar}(px)$,
- p_\circ $\text{tvar}(px) \approx \text{tvar}(p_\diamond x)$ and maximizing $\mathcal{M}(p, x)$,
- p_\star minimal $\text{tvar}(px)$,
- p_* maximal $\text{tvar}(px)$ (PCA).

4.2. Results. In Figure 4.1(b) we see the linear least squares fitting line, computed directly and via the slope and intercept as stated in (3.6) and (3.7). The correlation coefficient (2.13) is 0.98, which suggests that preserving the two properties is highly competing and needs to be balanced.

Method	NN (10 HU)	NN (5 HU)	SVM
original	97.6	97.5	96.7
p_{\diamond}	98.4	98.3	97.3
p_{\times}	88	87.9	87.6
p_{\square}	87.3	87	87.7
p_{\circ}	96.8	96.6	96
p_{*} (PCA)	96.9	96.9	96
p_{*}	61.5	59	56

TABLE 4.1. Classification results of iris data, when using projected input data in support vector machine (SVM) and shallow neural networks (NN).

In Table 4.1 the classification results are presented, where the results of the neural networks correspond to the mean of 1000 independent runs. We can see that in this comparison the projector p_{\diamond} yields the highest results, which corresponds to preserving $\mathcal{M}(p, x) \approx 1$ and maximizing $\text{tvar}(px)$. It even yields higher results than working with the original input data. The projections that preserve $\mathcal{M}(p, x) \approx 1$ but do not take care of the magnitude of the total variance yield worse results. On the other hand, the projections that just focus on high total variance still do not yield as high results as the projection p_{\diamond} that balances both properties.

Remark 4.1. *Heuristics in Remark 2.3 suggest random projectors for $k \ll d/2$ and PCA for $k \gg d/2$. Given a data set x , the projector p_{\diamond} is a good choice to balance both objectives O1) and O2) for $k \approx d/2$. For higher dimensions an accurate representation of $G_{k,d}$, in order to heuristically select p_{\diamond} , requires large computational costs.*

5. VARIATIONAL LOSS FUNCTIONS

In the previous section projectors were applied to input features of shallow neural networks. Since in more complex architectures, such as deep neural networks, the adaption of weights can be viewed as optimization of the input features, we will now use projections and features to yield beneficial representations of the output/target space.

Let the training data be input vectors $\{x_i\}_{i=1}^m \subset \mathbb{R}^r$ with associated target values $\{y_i\}_{i=1}^m \subset \mathbb{R}^s$. We consider training a neural network

$$f_{\theta} : \mathbb{R}^r \rightarrow \mathbb{R}^s,$$

where $\theta \in \mathbb{R}^N$ corresponds to the vector of all free parameters of a fixed architecture. In each optimization step for θ , the network's output $\{\hat{y}_i = f_{\theta}(x_i)\}_{i=1}^m \subset \mathbb{R}^s$ is compared with the targets $\{y_i\}_{i=1}^m$ via an underlying loss function L .

In contrast to ordinary learning problems with highly accurate target data, complicated learning tasks arising in many real world problems do not yield sufficient results when optimizing neural networks with standard loss

functions L , such as the widely used mean least squares error

$$(5.1) \quad L_{\text{MSE}}(\{y_i\}_{i=1}^m, \{\hat{y}_i\}_{i=1}^m) := \frac{1}{m} \sum_{i=1}^m \|y_i - \hat{y}_i\|^2.$$

The training data may contain important information that is often poorly represented within the original target data. To overcome this issue, we propose to add information tailored to the particular learning problem by modifying the loss function via additional features of the outputs and targets.

We select

$$T_j : \mathbb{R}^s \rightarrow \mathbb{R}^t, \quad j = 1, \dots, d,$$

where the transformed output $T_j(\hat{y}_i)$ and target values $T_j(y_i)$ represent additional information that is used in a variational loss function specified below. Note that T_j is not required to be linear. To facilitate the selection of the output features T_j for a specific learning problem, we shall allow for additional weighting. The previous sections suggest that orthogonal projections can provide favorable feature combinations, which essentially turns into a weighting procedure.

To enable suitable projections, we stack the output/target features

$$T(y_i) := \begin{pmatrix} T_1(y_i)^\top \\ \vdots \\ T_d(y_i)^\top \end{pmatrix} \in \mathbb{R}^{d \times t},$$

so that applying a projector $p \in \mathcal{G}_{k,d}$ to each column of $T(y_i)$ yields $p(T(y_i)) \in \mathbb{R}^{d \times t}$. We now define the modified loss function

$$(5.2) \quad L_p(\{y_i\}, \{\hat{y}_i\}) := L_1(\{y_i\}, \{\hat{y}_i\}) + \alpha \cdot L_2(\{p(T(y_i))\}_{i=1}^m, \{p(T(\hat{y}_i))\}_{i=1}^m),$$

where $\alpha > 0$ and L_1, L_2 correspond to conventional loss functions. Apparently, L_p depends on the choice of $p \in \mathcal{G}_{k,d}$. The projection $p(T(y_i))$ weighs the previously chosen feature transformations $T(y_i)$. Standard choices of L_1 and L_2 are L_{MSE} , in which case L_p becomes

$$(5.3) \quad L_p(\{y_i\}, \{\hat{y}_i\}) = \frac{1}{m} \sum_{i=1}^m \|y_i - \hat{y}_i\|^2 + \frac{\alpha}{m} \sum_{i=1}^m \|p(T(y_i)) - p(T(\hat{y}_i))\|_{\text{F}}^2.$$

Remark 5.1. For $k = d$, the projector p is the identity. In this case the transformation can map into different spaces, i.e.

$$T_j : \mathbb{R}^s \rightarrow \mathbb{R}^{t_j}, \quad j = 1, \dots, d,$$

and the second part of the loss function in (5.2) can be split into

$$(5.4) \quad L_2(\{T(y_i)\}_{i=1}^m, \{T(\hat{y}_i)\}_{i=1}^m) = \alpha \sum_{j=1}^d L_2^j(\{T_j(y_i)\}_{i=1}^m, \{T_j(\hat{y}_i)\}_{i=1}^m),$$

where L_2^1, \dots, L_2^d are standard loss functions.

It should be mentioned that α resembles a regularization parameter. The actual minimization of (5.1) among θ is usually performed through Tikhonov type regularization in many standard deep neural network implementations.

The variational formulation (5.2) adds one further variational step for beneficial output data representation.

Remark 5.2. *Our proposed structure with target feature maps T_1, \dots, T_d as in (5.4) relates to multi-task learning, which has been successfully used in deep neural networks [11]. It handles multiple learning problems with different outputs at the same time. In contrast to multi-task learning, we aim to solve a single problem, split output/target information by T_1, \dots, T_d , and rejoin via the projection.*

For the projected output in the variational loss function it is not possible to identify a balancing projection p heuristically (such as p_\diamond in Section 4), because the output changes in each iteration when the loss function is called. In the following clinical numerical experiment we overcome this issue by using random projections and PCA in each optimization step in comparison to the deterministic choice of projections from a t-design of a low-cardinality sequence, that covers the underlying space well.

6. APPLICATION TO CLINICAL IMAGE DATA

The first experiment is a clinical problem in retinal image analysis of the human eye, where the disruptions of the so-called photoreceptor layers need to be quantified in optical coherence tomography images (OCT). The photoreceptors have been identified as the most important retinal biomarker for prediction of vision from OCT in various clinical publications, see e.g. [21]. As OCT technology advances, clinicians are not able to look at each slice of OCT themselves (in mean they get 250 slices per patient and have 3-5 minutes/patients including their clinical examination). Therefore, automated classification of e.g. photoreceptor status is necessary for clinical guidance.

6.1. Data and objective. In this application, OCT images of different retinal diseases (diabetic macular edema and retinal vein occlusion) were provided by the Vienna Reading Center recorded with the Spectralis OCT device (Heidelberg Engineering, Heidelberg, Germany). Each patient's OCT volume consists of 49 cross-sections/slices (496×512 pixels) recorded in an area of 6×6 mm in the center of the human retina, which is the part of the retina responsible for vision. Each of the slices was manually annotated by a trained grader of the reading center. This is a challenging and time-consuming procedure that is not feasible in clinical routine but only in a research setting. The binary pixel-wise annotations serve as target values, enabling a supervised learning framework.

The objective is to accurately detect the photoreceptor layers and their disruptions pixel-wise in each OCT slice by training a deep convolutional neural network with a suitable loss function. The learning problem is complicated by potentially inaccurate target annotations, as studies have shown that inconsistencies between trained graders are common, cf. [32]. Moreover, the learning task is unbalanced in the sense that there are many more slices showing none or very little disruptions. We shall observe that optimization with respect to standard loss functions performs poorly in regards to detecting disruptions. The variational loss function proposed in the previous section can enhance the detection.

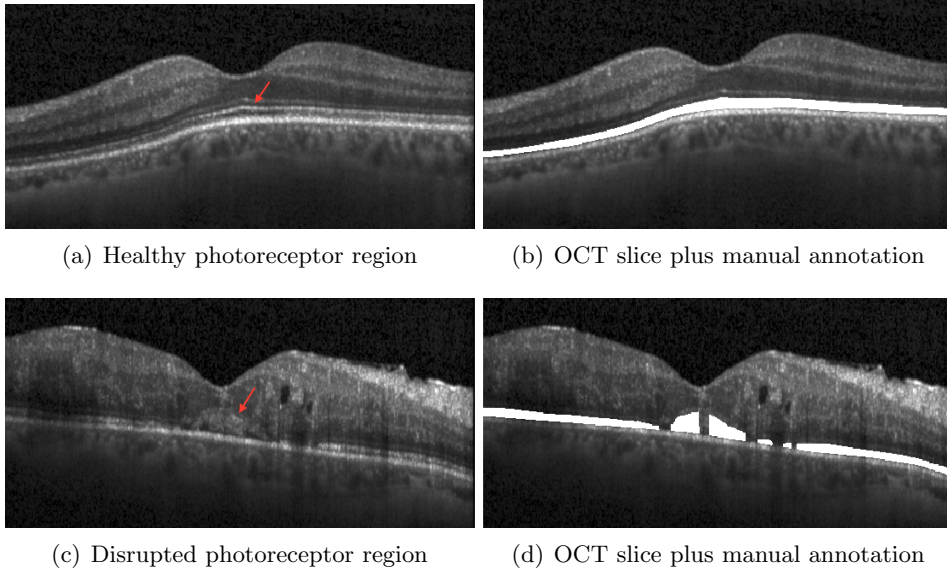


FIGURE 6.1. OCT provides cross-sectional visualization of the human retina.

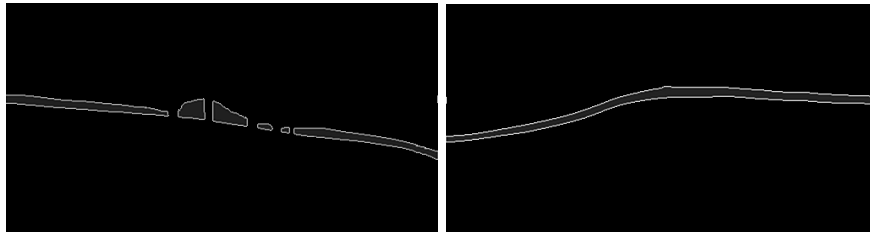
6.2. Convolutional neural network learning. We implemented our experiments using Python 3.6 with Pytorch 0.4.0. A deep convolutional neural network f_θ is trained by applying the U-Net architecture reported in [30] with a softmax activation function. A set of 20 OCT volumes (980 slices) from different patients with corresponding annotations are used for training, where 4 volumes were used for calibration (validation set). Another 2 independent test volumes were identified for evaluating the results, one without any disruptions in the photoreceptor layers, whereas the other one includes a high number of disruptions.

Each OCT slice is represented by a vector $x_i \in \mathbb{R}^r$ with $r = 496 \cdot 512$. The collection $\{x_i\}_{i=1}^m$ corresponds to all slices from the training volumes, i.e. $m = 20 \cdot 49$. Further matching the notation of the previous section, we have $r = s$ and $f_\theta : \mathbb{R}^r \rightarrow \mathbb{R}^r$ with binary target vectors $y_i \in \{0, 1\}^r$. We observe that disruptions are not identified reliably when using the least squared loss function (5.1). To overcome this issues, we use the proposed variational loss function with least squared losses as stated in (5.3).

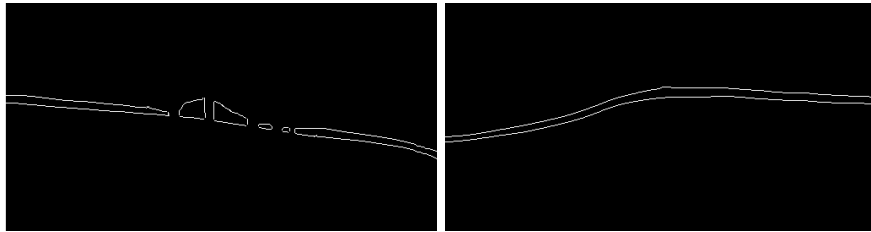
To enhance disruptions within the output/target space, we heuristically choose $d = 4$ local features derived from Shearlet coefficients ([25]) T_1 , a gradient filter (Prewitt) T_2 , a Gaussian highpass filter T_3 , and a Frangi Filter ([20]) T_4 applied to the binary images, see Figure 6.2. These feature transformations keep the same size, $T_j : \mathbb{R}^r \rightarrow \mathbb{R}^r$, for $j = 1, \dots, d$.

We can derive different variational loss functions L_p by choosing different $p \in \mathcal{G}_{k,d}$ for (5.2). In this experiment we use the following projections:

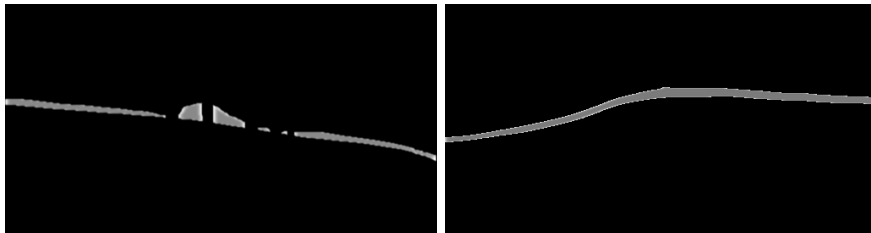
- $p = I_4$,
- $\{p_l\}_{l=1}^{15}$, all projections from a t-design of strength 2 $\subset \mathcal{G}_{2,4}$ (see [8]),
- $p_{\text{PCA}} \in \mathcal{G}_{2,4}$, projection determined by PCA for each batch,
- $p_{\lambda_{2,4}}$, random projection chosen according to $\lambda_{2,4}$ in each batch.



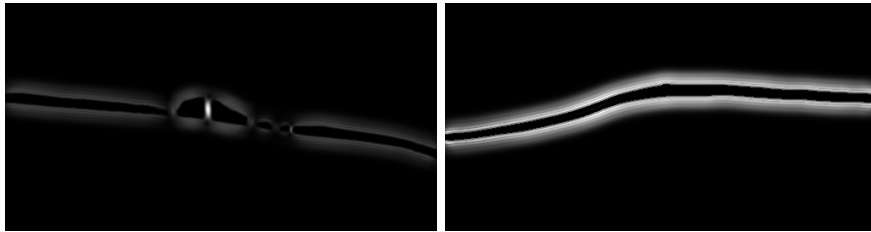
(a) Shearlet coefficients



(b) Prewitt



(c) Gaussian highpass



(d) Frangi filter

FIGURE 6.2. Output features that enhance edges in different ways. It is not obvious which transformations are of most importance, weighting by projections can overcome this issue.

6.3. Results. Since the detection problem is highly unbalanced we use precision/recall curves [13] for evaluating the overall performance of each loss function model. The area under the curve (AUC) was used as a numerical indicator of the success rate. The higher the AUC the better the classification.

The results of the different loss functions on the independent test set are stated in Table 6.1. Due to the unbalance within the data, the photoreceptor region is identified well, but disruptions are not identified reliably when

TABLE 6.1. Comparison of AUC values for photoreceptors segmentation and disruption detection.

Loss function	Photoreceptors	Disruptions
L_{MSE}	0.9724	0.3954
L_p		
$p = I_4$	0.9766	0.6045
$p_{\lambda_{2,4}}$	0.9796	0.5690
p_{PCA}	0.9734	0.5196
p_{12}	0.9755	0.6490

using the least squared loss function (5.1). For $\alpha = 0.5$ all proposed variational loss functions L_p immensely increase the success rate of the disruption quantification. The highest result was achieved by using the fixed projection p_{12} from the t-design sequence $\{p_l\}_{l=1}^{15}$ on the output/target features. This corresponds to the results of the previous sections, stating that depending on the particular data there are projections in the overall space acting beneficially. Since this projection generally cannot be found beforehand, using random projections or PCA in each loss function evaluation step is easier possible in practice. Random projections yield the highest overall accuracy and also beat PCA concerning the detection of disruptions.

In practice the choice of random projections in L_p seems beneficial. Random projections are fast to compute and generalize the added feature information. In the following we will view a second classification problem based on spectrograms, where variational loss functions with random projections can improve the accuracy.

7. APPLICATION TO MUSICAL DATA

Here, the learning task is a prototypical problem in Music Information Retrieval, namely multi-class classification of musical instruments. In analogy to the MNIST problem in image recognition, this classification problem is commonly used as a basis of comparison for innovative methods, since the ground truth is unambiguous and sufficient annotated data are available. The input to the neural network consists of spectrograms of audio signals, which is the standard choice in audio machine learning. Spectrograms are calculated from the time signal using a short-time Fourier transform and taking the absolute value squared of the resulting spectra, thus yielding a vector for each time-step and a two-dimensional array, like an image, cf. [15].

Reproducible code and more detailed information of our computational experiments can be found in the online repository [22].

7.1. Data and objective. The publicly available GoodSounds dataset [29] contains recordings of single notes and scales played by several single instruments. To gain equally balanced input classes we restrict the classification problem to 6 instruments: clarinet, flute, trumpet, violin, alto saxophone

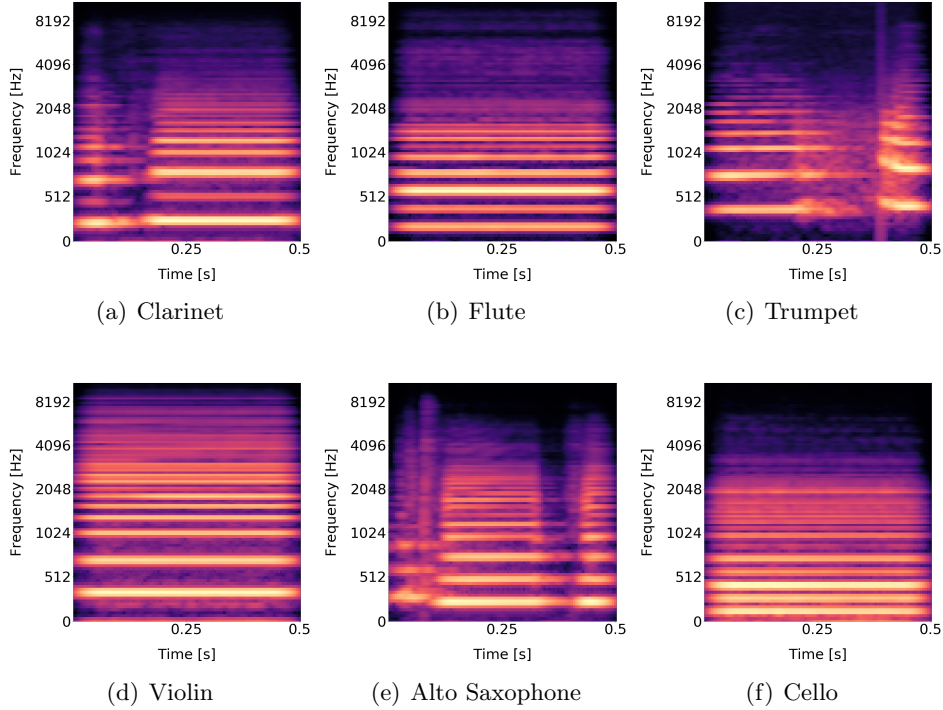


FIGURE 7.1. Log mel spectrograms of the 6 different instruments. Intensities range from zero (black) to 1 (yellow).

and cello. Note that the recordings are monophonic, so that each recording yields one spectrogram that we aim to correctly assign to one of the 6 instruments.

After removing the silence [3, 28], segments from the raw audio files are transformed into log mel spectrograms [17], so that we obtain images of time-frequency representations with size 100×100 . One example spectrogram for each class of instruments is depicted in Figure 7.1.

7.2. Convolutional neural network learning. We implemented a fully convolutional neural network $f_\theta : \mathbb{R}^r \rightarrow \{0, 1\}^s$, cf. [26], where $r = 100 \times 100$ and $s = 6$, in Python 3.6 using Keras 2.2.4 framework [18] and trained it on the Nvidia GTX 1080 Ti GPU. The data is split into 140 722 training, 36 000 validation and 36 000 independent test samples. We heuristically choose $d = 16$ feature transformations T_1, \dots, T_{16} arising directly from the particular output class, with $T_j : \{0, 1\}^6 \rightarrow \mathbb{R}$, for $j = 1, \dots, 16$. Amongst others the transformations are chosen from the enhanced scheme of taxonomy [33] and from the table of Frequencies, Harmonics and Under Tones [35]. We use the proposed variational loss function L_p (5.2), where L_1 corresponds to the categorical-cross-entropy loss [34] and L_2 to the mean squared error as in (5.3). We consider here two choices of p : the identity I_{16} and random projectors $p \sim \lambda_{6,16}$ in $\mathcal{G}_{6,16}$.

The deep learning model is sensitive to various hyper-parameters, including α and p , in addition to conventional parameters, such as the number of convolutional kernels, learning rate and the parameter β for Tikhonov

α	β	p	training	test data
0	0	-	0.5541	0.5716
0.01	0	I_{16}	0.5650	0.5683
0.01	0	$p_{\lambda_{6,16}}$	0.7722	0.7657
0	0.05	-	0.9771	0.9729
0.01	0.05	I_{16}	0.9849	0.9802
0.01	0.05	$p_{\lambda_{6,16}}$	0.9857	0.9833

TABLE 7.1. Classification results with different parameter choices. The standard inbuilt Tikhonov regularization (ℓ_2 -norm of θ) is weighted by β . For $\alpha > 0$ the feature transformations $\{T_j\}_{j=1}^{16}$ are used in the loss function, either directly or weighted by a random projection $p_{\lambda_{6,16}}$. The accuracy of the model is measured by the number of correctly classified samples divided by the number of all samples.

regularization. To find the best choices in a fair trial we utilize a random hyper-parameter search approach, where we train 60 models and select the 3 best ones for a more precise search over different α in the variational loss function and β for Tikhonov regularization. This results in 212 models that are evaluated on the training and validation set. Finally, we select the best model based on the accuracy of the validation set and evaluate it on the independent test set. For comparison we also evaluate this model with no Tikhonov regularization, i.e. $\beta = 0$, see Table 7.1.

7.3. Results. Table 7.1 shows that no regularization and no features provide the poorest results. It seems that adding features with random projections have a regularizing effect and improve the results significantly. As expected, it is important to include Tikhonov regularization on θ to advance the results. Further enhancement happens by adding features via the modified variational loss function with or without additional weighting from projections. All results are very stable and are generalizing very well from training to the independent test set, see [22] for further details.

8. ACKNOWLEDGMENT

This work was partially funded by the Vienna Science and Technology Fund (WWTF) through project VRG12-009, by WWTF AugUniWien/FA746A0249, by International Mobility of Researchers (CZ.02.2.69/0.0/0.0/16 027/0008371), and by project LO1401. For the research, infrastructure of the SIX Center was used.

APPENDIX A. PROOF OF THEOREM 2.5

A.1. **Proof of (2.14) in Theorem 2.5.** For $\{y_i\}_{i=1}^M \subset \mathbb{R}^d$ and $p \in \mathcal{G}_{k,d}$, we define

$$(A.1) \quad f(p, \{y_i\}_{i=1}^M) := \frac{1}{M} \sum_{i=1}^M \frac{d}{k} \|p(y_i)\|^2.$$

Given two sets, $\{y_i\}_{i=1}^{M_1}, \{z_j\}_{j=1}^{M_2} \subset \mathbb{R}^d$, suppose that $P \in \mathcal{G}_{k,d}$ is a random matrix, distributed according to a cubature measure of strength at least 2. The covariance is given by

$$\begin{aligned} \text{Cov}(f(P, \{y_i\}_{i=1}^{M_1}), f(P, \{z_j\}_{j=1}^{M_2})) &= \\ \mathbb{E}[(f(P, \{y_i\}) - \mathbb{E}[f(P, \{y_i\})])(f(P, \{z_j\}) - \mathbb{E}[f(P, \{z_j\})])] \end{aligned}$$

Using the identity, cf. [2],

$$(A.2) \quad \frac{d}{k} \mathbb{E}[\|Py\|^2] = \|y\|^2,$$

directly yields

$$\begin{aligned} \text{Cov}(f(P, \{y_i\}_{i=1}^{M_1}), f(P, \{z_j\}_{j=1}^{M_2})) &= \\ \mathbb{E}[(\frac{1}{M_1} \sum_{i=1}^{M_1} \frac{d}{k} \|P(y_i)\|^2 - \frac{1}{M_1} \sum_{i=1}^{M_1} \|y_i\|^2)(\frac{1}{M_2} \sum_{i=1}^{M_2} \frac{d}{k} \|P(z_i)\|^2 - \frac{1}{M_2} \sum_{i=1}^{M_2} \|z_i\|^2)] \end{aligned}$$

Following [6, Theorem 2.4, Section 3.1] we use that

$$(A.3) \quad \mathbb{E}[\|Py\|^2 \|Pz\|^2] = \frac{1}{q}(\alpha_1 \|y\|^2 \|z\|^2 + \alpha_2 \langle y, z \rangle^2), \quad y, z \in \mathbb{R}^d,$$

holds, where $q = (d-1)d(d+2)$, $\alpha_1 = (d+1)k^2 - 2k$ and $\alpha_2 = 2k(d-k)$. This leads to the explicit formula of the population covariance

$$(A.4) \quad \begin{aligned} \text{Cov}(f(P, \{y_i\}_{i=1}^{M_1}), f(P, \{z_j\}_{j=1}^{M_2})) &= \\ \frac{a_{k,d}}{M_1 M_2} \sum_{i=1}^{M_1} \sum_{j=1}^{M_2} \langle y_i, z_j \rangle^2 - \frac{a_{k,d}}{d} \left(\frac{1}{M_1} \sum_{i=1}^{M_1} \|y_i\|^2 \right) \left(\frac{1}{M_2} \sum_{j=1}^{M_2} \|z_j\|^2 \right), \end{aligned}$$

with $a_{k,d} = \frac{2d(d-k)}{k(d-1)(d+2)}$.

For $y := \{y_i\}_{i=1}^M \subset \mathbb{R}^d \setminus \{0\}$ we set $\hat{y}_i := \frac{y_i}{\|y_i\|}$, for $i = 1, \dots, M$. The identity (A.4) enables us to compute the population correlation

$$(A.5) \quad \text{Corr}(f(P, y), f(P, \hat{y})) = \frac{\text{Cov}(f(P, y), f(P, \hat{y}))}{\sqrt{\text{Var}(f(P, y))} \sqrt{\text{Var}(f(P, \hat{y}))}}$$

by the explicit formulas

$$\begin{aligned} \text{Cov}[f(P, y), f(P, \hat{y})] &= \frac{a_{k,d}}{M^2} \sum_{i,j=1}^M \langle y_i, \hat{y}_j \rangle^2 - \frac{a_{k,d}}{d} \cdot \frac{1}{M} \sum_{i=1}^M \|y_i\|^2 \\ \text{Cov}[f(P, y), f(P, y)] &= \text{Var}[f(P, y)] = \frac{a_{k,d}}{M^2} \sum_{i,j=1}^M \langle y_i, y_j \rangle^2 - \frac{a_{k,d}}{d} \left(\frac{1}{M} \sum_{i=1}^M \|y_i\|^2 \right)^2 \end{aligned}$$

$$\text{Cov} [f(P, \hat{y}), f(P, \hat{y})] = \text{Var}[f(P, \hat{y})] = \frac{a_{k,d}}{M^2} \sum_{i,j=1}^M \langle \hat{y}_i, \hat{y}_j \rangle^2 - \frac{a_{k,d}}{d}.$$

Since the variance is always nonnegative and $\frac{a_{k,d}}{d} > 0$, the denominator of $\text{Corr}(f(P, y), f(P, \hat{y}))$ in (A.5) satisfies

$$\begin{aligned} \sqrt{\text{Var}(f(P, y))} \sqrt{\text{Var}(f(P, \hat{y}))} &\leq \sqrt{\left(\frac{a_{k,d}}{M^2} \sum_{i,j=1}^M \langle y_i, y_j \rangle^2 \right) \left(\frac{a_{k,d}}{M^2} \sum_{i,j=1}^M \langle \hat{y}_i, \hat{y}_j \rangle^2 \right)} \\ &\leq \frac{a_{k,d}}{M^2} \sqrt{\left(\sum_{i,j=1}^M \langle y_i, y_j \rangle^2 \right) \left(\frac{1}{\min_i (\|y_i\|)^4} \sum_{i,j=1}^M \langle y_i, y_j \rangle^2 \right)} \\ &\leq \frac{1}{\min_i (\|y_i\|)^2} \frac{a_{k,d}}{M^2} \sum_{i,j=1}^M \langle y_i, y_j \rangle^2. \end{aligned}$$

The numerator of $\text{Corr}(f(P, y), f(P, \hat{y}))$ in (A.5) is estimated by

$$\text{Cov}(f(P, y), f(P, \hat{y})) \geq \frac{a_{k,d}}{\max_i (\|y_i\|)^2} \frac{1}{M^2} \sum_{i,j=1}^M \langle y_i, y_j \rangle^2 - \frac{a_{k,d}}{d} \max_i (\|y_i\|)^2$$

For $d \geq M$, a short calculation yields $\text{Cov}(f(P, y), f(P, \hat{y})) \geq 0$, so that we obtain

$$\text{Corr}(f(P, y), f(P, \hat{y})) \geq \frac{\min_i (\|y_i\|)^2}{\max_i (\|y_i\|)^2} - \frac{\min_i (\|y_i\|)^2 \max_i (\|y_i\|)^2}{\frac{d}{M^2} \sum_{i,j=1}^M \langle y_i, y_j \rangle^2}.$$

The lower bound $\sum_{i,j=1}^M \langle y_i, y_j \rangle^2 \geq M \min_i (\|y_i\|)^4$ yields

$$\text{Corr}(f(P, y), f(P, \hat{y})) \geq \frac{\min_i (\|y_i\|)^2}{\max_i (\|y_i\|)^2} - \frac{M}{d} \cdot \frac{\max_i (\|y_i\|)^2}{\min_i (\|y_i\|)^2}.$$

Since the correlation is scaling invariant the choice $y = \{x_i - x_j : 1 \leq i < j \leq m\}$ with $M = \frac{m(m-1)}{2}$ implies (2.14) in Theorem 2.5. Incorporating the correct scaling yields the following corollary:

Corollary A.1. *For a given data set $x = \{x_i\}_{i=1}^m$ and for random $P \in \mathcal{G}_{k,d}$ the (co)variances of $\text{tvar}(Px)$ (2.4) and $\mathcal{M}(P, x)$ (2.8) are given by*

$$\begin{aligned} \text{Cov}(\mathcal{M}(P, x), \text{tvar}(Px)) &= \frac{k}{2d} \left(\frac{a_{k,d}}{M^2} \sum_{i<j} \sum_{l<r} \langle x_i - x_j, \frac{x_l - x_r}{\|x_l - x_r\|} \rangle^2 - \frac{a_{k,d}}{d} \cdot \frac{1}{M} \sum_{i<j} \|x_i - x_j\|^2 \right), \\ \text{Var}(\text{tvar}(Px)) &= \frac{k^2}{4d^2} \left(\frac{a_{k,d}}{M^2} \sum_{i<j} \sum_{l<r} \langle x_i - x_j, x_l - x_r \rangle^2 - \frac{a_{k,d}}{d} \left(\frac{1}{M} \sum_{i<j} \|x_i - x_j\|^2 \right)^2 \right), \\ \text{Var}(\mathcal{M}(P, x)) &= \frac{a_{k,d}}{M^2} \sum_{i<j} \sum_{l<r} \left\langle \frac{x_i - x_j}{\|x_i - x_j\|}, \frac{x_l - x_r}{\|x_l - x_r\|} \right\rangle^2 - \frac{a_{k,d}}{d}, \end{aligned}$$

where $M = \frac{m(m-1)}{2}$ and $a_{k,d} = \frac{2d(d-k)}{k(d-1)(d+2)}$.

A.2. Proof of the second part of Theorem 2.5. For fixed parameters $\mu > 0, \sigma^2 > 0$, that do not depend on d , let $Y_1 \in \mathbb{R}^d$ be a random vector, whose squared entries are independent, identically distributed with mean $\mathbb{E}Y_{1,l}^2 = \mu$ and variance $\text{Var}(Y_{1,l}^2) = \sigma^2$, for $l = 1, \dots, d$. We immediately observe

$$\mathbb{E}\left(\frac{\|Y_1\|^2}{\sqrt{d}}\right) = \sqrt{d}\mu, \quad \text{Var}\left(\frac{\|Y_1\|^2}{\sqrt{d}}\right) = \sigma^2.$$

For any $c > 0$, Chebychev's inequality yields

$$\mathbb{P}\left(\left|\frac{\|Y_1\|^2}{\sqrt{d}} - \sqrt{d}\mu\right| \geq c\sigma\right) \leq \frac{1}{c^2}.$$

Suppose that Y_2, \dots, Y_M are copies of Y_1 , not necessarily independent. Then the union bound

$$\mathbb{P}\left(\left|\frac{\|Y_i\|^2}{\sqrt{d}} - \sqrt{d}\mu\right| \geq c\sigma, \text{ for some } i = 1, \dots, M\right) \leq \frac{M}{c^2}$$

implies that

$$\sqrt{d}\mu - c\sigma \leq \frac{\min_i(\|Y_i\|)^2}{\sqrt{d}} \leq \frac{\max_i(\|Y_i\|)^2}{\sqrt{d}} \leq \sqrt{d}\mu + c\sigma$$

holds with probability at least $1 - \frac{M}{c^2}$. Provided that $\sqrt{d}\mu \neq c\sigma$ and $0 < \sqrt{d}\mu - c\sigma$, we deduce

$$\frac{\sqrt{d}\mu - c\sigma}{\sqrt{d}\mu + c\sigma} \leq \frac{\min_i(\|Y_i\|)^2}{\max_i(\|Y_i\|)^2} \leq \frac{\sqrt{d}\mu + c\sigma}{\sqrt{d}\mu - c\sigma}.$$

We can choose $c = \frac{\mu}{\sigma} \sqrt[4]{d}$, since $0 < c \leq \frac{\sqrt{d}\mu}{\sigma} \leq \frac{\sqrt{d}\mu}{\sigma}$. That directly yields

$$\frac{1 - \frac{1}{\sqrt[4]{d}}}{1 + \frac{1}{\sqrt[4]{d}}} \leq \frac{\min_i(\|Y_i\|)^2}{\max_i(\|Y_i\|)^2} \leq \frac{1 + \frac{1}{\sqrt[4]{d}}}{1 - \frac{1}{\sqrt[4]{d}}}$$

holds with probability at least $1 - \frac{\mu^2 M}{\sigma^2 \sqrt{d}}$.

It follows directly that $\frac{\min_i(\|Y_i\|)^2}{\max_i(\|Y_i\|)^2}$ converges towards 1 in probability for $d \rightarrow \infty$,

The choice $\{Y_1, \dots, Y_M\} = \{X_i - X_j : 1 \leq i < j \leq m\}$ implies the second part of Theorem 2.5.

A.3. Calculations for population covariances. We notice that $\|p(x_i - x_j)\|^2 = \text{trace}(px_i x_i^\top - px_j x_j^\top)$ is a polynomial of degree 1 in p . Hence, $\text{tvar}(px)$ in (2.4) is also a polynomial of degree 1 in p . If $\{p_l\}_{l=1}^n$ is a 1-design, then the sample mean of $\{\text{tvar}(p_1 x), \dots, \text{tvar}(p_n x)\}$ satisfies

$$\frac{1}{n} \sum_{l=1}^n \text{tvar}(p_l x) = \mathbb{E} \text{tvar}(P x),$$

which is the population mean of $\text{tvar}(P x)$, with $P \sim \lambda_{k,d}$. Similarly, the term $\|p(x_i - x_j)\|^4$ is a polynomial of degree 2 in p , so that $(\mathcal{M}(p, x))^2$ in (2.8) is a polynomial of degree 2 in p . If $\{p_l\}_{l=1}^n$ is a 2-design, then we derive

$$\sum_{l=1}^n (\mathcal{M}(p_l, x))^2 - \left(\sum_{j=1}^n \mathcal{M}(p_l, x)\right)^2 = \mathbb{E}(\mathcal{M}(P, x))^2 - \mathbb{E}\left(\sum_{j=1}^n \mathcal{M}(P, x)\right)^2,$$

with $P \sim \lambda_{k,d}$. In other words, the sample variance of $\{\mathcal{M}(p_1, x), \dots, \mathcal{M}(p_n, x)\}$ coincides with the population variance $\text{Var}(\mathcal{M}(P, x))$. Analogously, we deduce that the sample covariance of (3.5) coincides with the population covariance $\text{Cov}(\mathcal{M}(P, x), \text{tvar}(Px))$ with $P \sim \lambda_{k,d}$.

REFERENCES

1. D. Achlioptas, *Database-friendly random projections: Johnson-Lindenstrauss with binary coins*, Journal of Computer and System Sciences **66** (2003), no. 4, 671–687.
2. C. Bachoc and M. Ehler, *Tight p -fusion frames*, Appl. Comput. Harmon. Anal. **35** (2013), no. 1, 1–15.
3. C. Bagwell, *SoX - Sound Exchange the swiss army knife of sound processing.*, <https://launchpad.net/ubuntu/+source/sox/14.4.1-5>, Accessed: 2018-10-31.
4. R. Baraniuk, M. Davenport, R. DeVore, and M. Wakin, *A simple proof of the restricted isometry property for random matrices*, Constr. Approx. **28** (2008), no. 3, 253–263.
5. R. G. Baraniuk and M. B. Wakin, *Random projections of smooth manifolds*, Foundations of Computational Mathematics, vol. 9, 2006, pp. 941–944.
6. B. Bodman, M. Ehler, and M. Gräf, *From low to high-dimensional moments without magic*, J. Theor. Probab. (2017).
7. A. Breger, M. Ehler, H. Bogunovic, S. M. Waldstein, A. Philip, U. Schmidt-Erfurth, and B. S. Gerendas, *Supervised learning and dimension reduction techniques for quantification of retinal fluid in optical coherence tomography images*, Eye, Springer Nature (2017).
8. A. Breger, M. Ehler, and M. Gräf, *Quasi Monte Carlo integration and kernel-based function approximation on Grassmannians*, Frames and Other Bases in Abstract and Function Spaces, Applied and Numerical Harmonic Analysis series (ANHA), Birkhauser/Springer (2017).
9. A. Breger, M. Ehler, and M. Gräf, *Points on manifolds with asymptotically optimal covering radius*, Journal of Complexity **48** (2018), 1–14.
10. E. J. Candès and T. Tao, *Decoding by linear programming*, IEEE Trans. Inform. Theory **51** (2005), no. 12, 4203–4215.
11. R. Caruana, *Multitask learning*, Machine Learning **28** (1997), no. 1, 41–75.
12. S. Dasgupta and A. Gupta, *An elementary proof of a theorem of Johnson and Lindenstrauss*, Random Structures & Algorithms **22** (2003), no. 1, 60–65.
13. J. Davis and M. Goadrich, *The relationship between precision-recall and roc curves*, Proceedings of the 23rd International Conference on Machine Learning (New York, NY, USA), ICML '06, ACM, 2006, pp. 233–240.
14. P. de la Harpe and C. Pache, *Cubature formulas, geometrical designs, reproducing kernels, and Markov operators*, Infinite groups: geometric, combinatorial and dynamical aspects (Basel), vol. 248, Birkhäuser, 2005, pp. 219–267.
15. M. Dörfler, R. Bammer, and T. Grill, *Inside the spectrogram: Convolutional neural networks in audio processing*, IEEE International Conference on Sampling Theory and Applications (SampTA) (2017), 152–155.
16. M. Dörfler, T. Grill, R. Bammer, and A. Flexer, *Basic filters for convolutional neural networks applied to music: Training or design*, Neural Comput. & Applications (2018), 1–14.
17. B. McFee et al., *Librosa: 0.6.2*, <https://doi.org/10.5281/zenodo.1342708>, 2018.
18. F. Chollet et al., *Keras*, <https://keras.io>, 2015.
19. U. Etayo, J. Marzo, and J. Ortega-Cerdà, *Asymptotically optimal designs on compact algebraic manifolds*, J. Monatsh. Math. **186** (2018), no. 2, 235–248.
20. A.F. Frangi, W.J. Niessen, K.L. Vincken, and M.A. Viergever, *Multiscale vessel enhancement filtering*, Lecture Notes in Computer Science **1496** (1998).
21. B.S. Gerendas, X. Hu, A. Kaider, A. Montuoro, A. Sadeghipour, S.M. Waldstein, and U. Schmidt-Erfurth, *Oct biomarkers predictive for visual acuity in patients with diabetic macular edema*, Investigative Ophthalmology & Visual Science **58** (2017), no. 8, 2026–2026.
22. P. Harar, *Orthovar*, <https://gitlab.com/hararticles/orthovar>, 2018.

23. C. Hedge, A. C. Sankaranarayanan, W. Yin, and R. G. Baraniuk, *Numax: A convex approach for learning near-isometric linear embeddings*, IEEE Transactions on Signal Processing **83** (2015).
24. F. Kraahmer and R. Ward, *New and improved Johnson Lindenstrauss embeddings via the restricted isometry property*, SIAM Journal on Mathematical Analysis **43** (2011), no. 3, 1269–1281.
25. G. Kutyniok, W.-Q. Lim, and R. Reisenhofer, *Shearlab 3d: Faithful digital shearlet transforms based on compactly supported shearlets*, ACM Trans. Math. Softw. **42** (2016, www.shearlab.org).
26. J. Long, E. Shelhamer, and T. Darrell, *Fully convolutional networks for semantic segmentation*, Proceedings of the IEEE conference on computer vision and pattern recognition, 2015, pp. 3431–3440.
27. J. Matousek, *On variants of the Johnson-Lindenstrauss lemma*, Random Structures & Algorithms **33** (2008), no. 2, 142–156.
28. J. Navarrete, *The sox of silence*, <https://digitalcardboard.com/blog/2009/08/25/the-sox-of-silence>, 2009.
29. O. Romani Picas, H. Parra Rodriguez, D. Dabiri, H. Tokuda, W. Hariya, K. Oishi, and X. Serra, *A real-time system for measuring sound goodness in instrumental sounds*, Audio Engineering Society Convention 138, Audio Engineering Society, 2015.
30. O. Ronneberger, P. Fischer, and T. Brox, *U-net: Convolutional networks for biomedical image segmentation*, arxiv:1505.04597 (2015).
31. M. Udell, *Generalized low rank models*, Ph.D. thesis, Stanford University, 2015.
32. E. S. Varnousfaderani, J. Wu, W.-D. Vogl, A.-M. Philip, A. Montuoro, R. Leitner, C. Simader, S. M. Waldstein, B. S. Gerendas, and U. Schmidt-Erfurth, *A novel benchmark model for intelligent annotation of spectral-domain optical coherence tomography scans using the example of cyst annotation*, Computer Methods and Programs in Biomedicine **130** (2016), 93–105.
33. E.M. von Hornbostel and C. Sachs, *Classification of musical instruments: Translated from the original german by anthony baines and klaus p. wachsmann*, The Galpin Society Journal (1961), 3–29.
34. Z. Zhang and M. Sabuncu, *Generalized cross entropy loss for training deep neural networks with noisy labels*, Advances in Neural Information Processing Systems (NIPS) **31** (2018).
35. Inc. ZyTrax, *Frequency ranges*, <http://www.zytrax.com/tech/audio/audio.html>, 2018.